Electronic Supporting Information

Thiacalix[4]arene-supported heterodinuclear Ni^{II}-Ln^{III} complexes: slow magnetic relaxation behavior in dysprosium analogue

Jing-Yuan Ge, Jia-Ze Xie, Zhuang-Yu Zhao, Jing Ru, You Song, Jing-Lin Zuo*

State Key Laboratory of Coordination Chemistry, School of Chemistry and Chemical Engineering, Collaborative Innovation Center of Advanced Microstructures, Nanjing University, Nanjing 210093, P. R. China

* To whom correspondence should be addressed. Email: zuojl@nju.edu.cn; Fax: +86-25-83314502.

Nanjing University.

Caption of Content

13. **Fig. S9** The XRPD pattern of complex **3′** is consistent with that of complex **3**.
14. **Fig. S10** Frequency-dependent in-phase χ' and out-of-phase χ'' ac susceptibility signals for **3′** at the indicated frequencies under zero dc field.
15. **Fig. S11** Cole-Cole plots for **3′** under zero dc field. The solid lines represent the fit to the Debye model at the indicated temperatures.
16. **Fig. S12** Temperature-dependent in-phase χ' and out-of-phase χ'' ac susceptibility signals for **2** at the frequency of 999 Hz under zero dc field.
17. **Fig. S13** Temperature-dependent in-phase χ' and out-of-phase χ'' ac susceptibility signals for **2** at the frequency of 999 Hz under 800 Oe dc field.

Table S1. Selected bond angles (°) for **1**–**3**

	1 (Gd)	**2 (Tb)**	**3 (Dy)**
O(5)-Ln(1)-O(7)	101.98(12)	101.72(14)	102.05(10)
O(5)-Ln(1)-O(3)	169.22(12)	169.45(14)	169.55(10)
O(7)-Ln(1)-O(3)	86.39(11)	86.39(14)	86.06(9)
O(5)-Ln(1)-O(1)	106.61(12)	106.78(14)	106.16(9)
O(7)-Ln(1)-O(1)	134.18(11)	134.15(14)	134.35(9)
O(3)-Ln(1)-O(1)	71.06(11)	71.06(13)	71.59(9)
O(5)-Ln(1)-O(8)	92.88(12)	92.76(14)	92.63(9)
O(7)-Ln(1)-O(8)	141.69(12)	141.61(14)	141.82(10)
O(3)-Ln(1)-O(8)	76.36(11)	76.72(13)	76.95(9)
O(1)-Ln(1)-O(8)	71.69(11)	72.07(13)	71.76(9)
O(5)-Ln(1)-O(4)	81.38(11)	81.26(13)	81.48(9)
O(7)-Ln(1)-O(4)	79.50(11)	79.67(13)	79.44(9)
O(3)-Ln(1)-O(4)	107.08(10)	107.06(13)	106.74(9)
O(1)-Ln(1)-O(4)	70.45(10)	70.25(12)	70.27(8)
O(8)-Ln(1)-O(4)	138.11(11)	138.12(13)	138.08(9)
O(5)-Ln(1)-O(6)	78.73(11)	78.88(13)	79.06(9)
O(7)-Ln(1)-O(6)	78.33(11)	78.25(13)	78.57(9)
O(3)-Ln(1)-O(6)	96.57(11)	96.44(13)	96.34(9)
O(1)-Ln(1)-O(6)	141.71(10)	141.77(13)	141.43(9)
O(8)-Ln(1)-O(6)	70.17(11)	69.89(13)	69.82(9)
O(4)-Ln(1)-O(6)	146.27(9)	146.45(11)	146.72(8)
N(1)-Ni(1)-N(2)	87.23(16)	87.40(19)	87.11(13)
N(1)-Ni(1)-O(2)	98.00(16)	98.15(18)	98.10(13)
N(2)-Ni(1)-O(2)	90.01(15)	89.84(17)	90.05(12)
N(1)-Ni(1)-O(3)	169.11(15)	168.95(18)	168.56(12)
N(2)-Ni(1)-O(3)	102.31(15)	102.18(17)	102.87(12)
O(2)-Ni(1)-O(3)	87.36(13)	87.48(15)	87.60(11)
N(1)-Ni(1)-O(1)	88.42(15)	88.30(17)	88.59(12)
N(2)-Ni(1)-O(1)	173.57(15)	173.64(17)	173.47(12)
O(2)-Ni(1)-O(1)	85.91(13)	86.12(15)	85.69(10)
O(3)-Ni(1)-O(1)	82.48(13)	82.57(14)	81.93(10)
N(1)-Ni(1)-N(3)	90.14(17)	90.1(2)	90.13(14)

N(2)-Ni(1)-N(3)	83.86(16)	83.87(19)	83.84(13)
O(2)-Ni(1)-N(3)	169.58(16)	169.41(17)	169.50(12)
O(3)-Ni(1)-N(3)	85.74(15)	85.54(17)	85.46(12)
O(1)-Ni(1)-N(3)	100.88(14)	100.83(17)	101.09(11)
Ni(1)-O(1)-Ln(1)	102.77(13)	102.39(15)	102.40(10)
Ni(1)-O(3)-Ln(1)	103.61(14)	103.90(16)	103.98(11)

Table S2. Fitting of the Cole-Cole plots for **3** with a generalized Debye model in the temperature range 1.9–5.0 K under 800 Oe dc field

T / K	χ_S / cm^3 mol^{-1}	χ_T / cm^3 mol^{-1}	ln(τ / s)	α
1.9	0.734	9.954	-4.663	0.167
2.2	0.769	8.672	-5.517	0.133
2.5	0.809	7.762	-6.152	0.113
2.8	0.829	7.013	-6.650	0.099
3.3	0.841	6.005	-7.284	0.082
3.8	0.830	5.237	-7.746	0.073
4.5	0.801	4.404	-8.227	0.064
5.0	0.741	3.939	-8.510	0.062

Table S3. Fitting of the Cole-Cole plots for **3′** with a generalized Debye model in the temperature range 1.9–3.4 K under zero dc field

T / K	χ_S / cm^3 mol^{-1}	χ_T / cm^3 mol^{-1}	ln(τ / s)	α
1.9	0.547	0.870	-5.932	0.239
2.2	0.497	0.768	-6.532	0.181
2.5	0.454	0.686	-7.038	0.146
2.8	0.417	0.622	-7.451	0.127
3.1	0.386	0.567	-7.802	0.109
3.4	0.357	0.521	-8.103	0.108

Table S4. Shape analysis for the metal centers of **3**

ML7	PBPY-7	COC-7	CTPR-7	JPBPY-7
Dy1	**3.137**	3.687	3.258	5.505

PBPY-7 (D5h): Pentagonal bipyramid COC-7 (C3v): Capped octahedron

CTPR-7 (C2v): Capped trigonal prism JPBPY-7 (D5h): Johnson pentagonal bipyramid J13

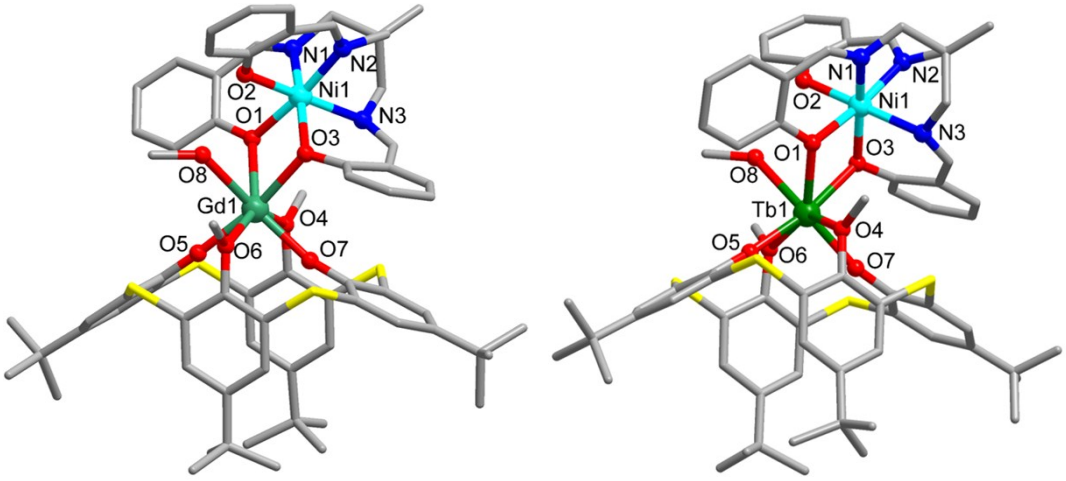

Fig. S1 Left: crystal structure of complex [(NiL_1)Gd(L_2)(CH_3OH)]·acetone (**1**). Right: crystal structure of complex [(NiL_1)Tb(L_2)(CH_3OH)]·acetone (**2**). Hydrogen atoms and uncoordinated solvents are omitted for clarity. (Ln green, Ni turquoise, S yellow, O red, N blue and C gray)

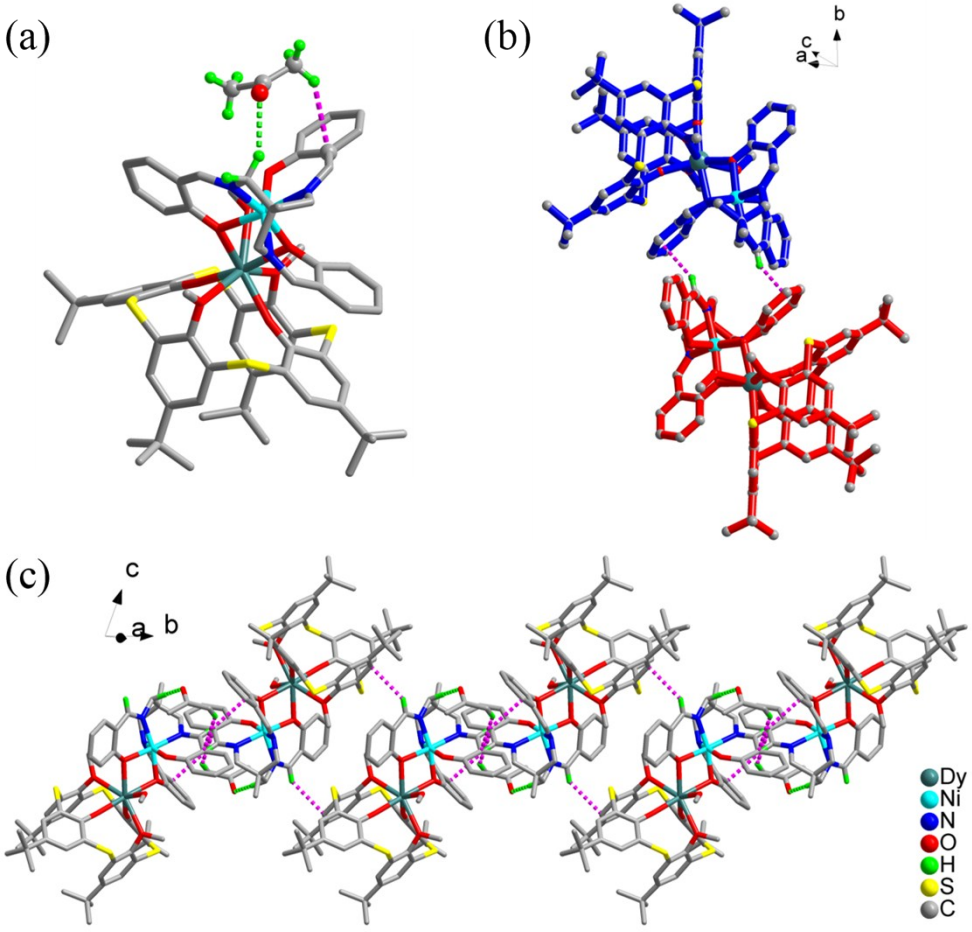

Fig. S2 (a) acetone molecule connects to the Ni^{II}-Dy^{III} clusters *via* weak C−H···O (green dashed line) and C−H···π (pink dashed line) interactions (b) Every two

neighbouring clusters are linked together to give a dimer through C−H···π interaction between solvent and the framework in **3**. (c) C−H···π interactions drive the dimers to a 1D chain along *b* axis.

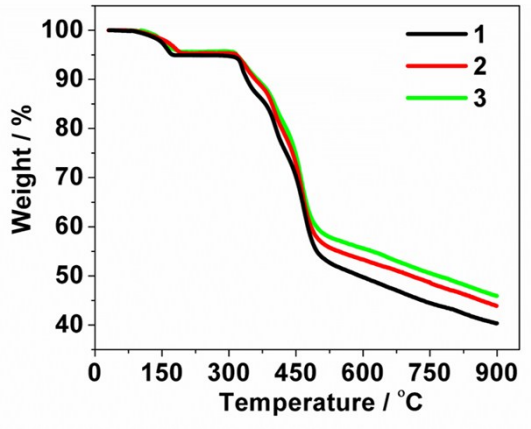

Fig. S3 TGA curves for complexes **1**–**3**.

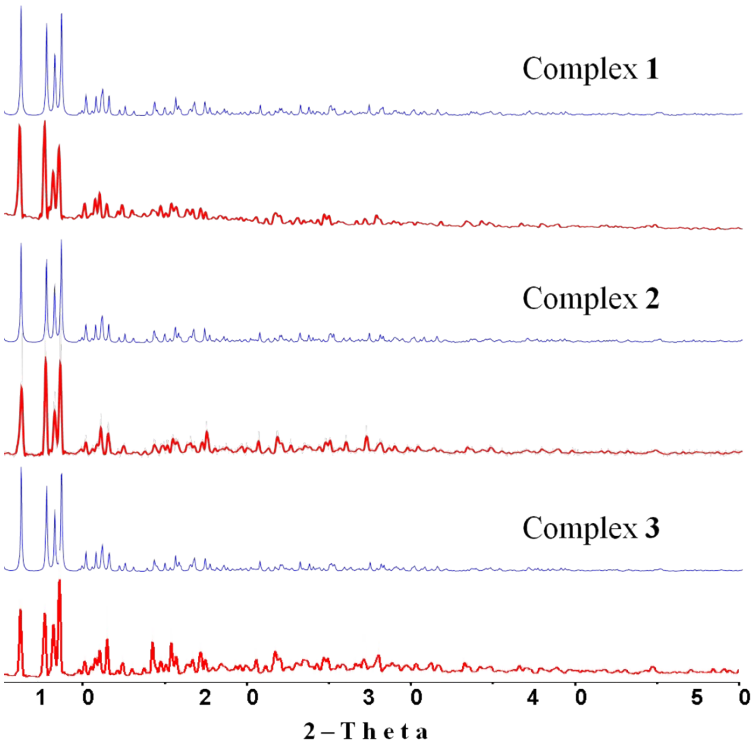

Fig. S4 The XRPD patterns (red lines) obtained from the as-synthesized solids of **1**–**3** and the simulated XRPD patterns (blue lines) from single crystals of **1**–**3**.

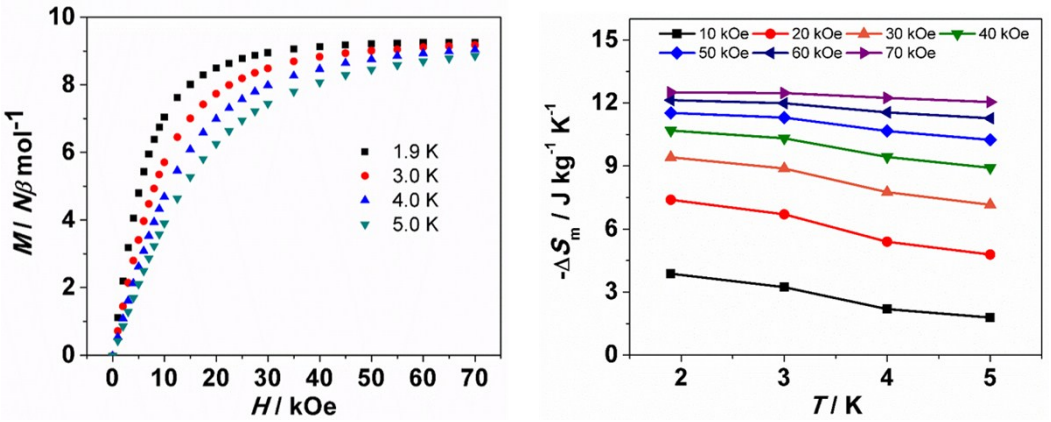

Fig. S5 Left: field-dependent magnetizations for **1** at T = 1.9−5.0 K and H = 0−70 kOe. Right: temperature dependence of magnetic entropy change ($-\Delta S_m$) as calculated from the magnetization data of **1** at T = 1.9−5.0 K and 0−70 kOe.

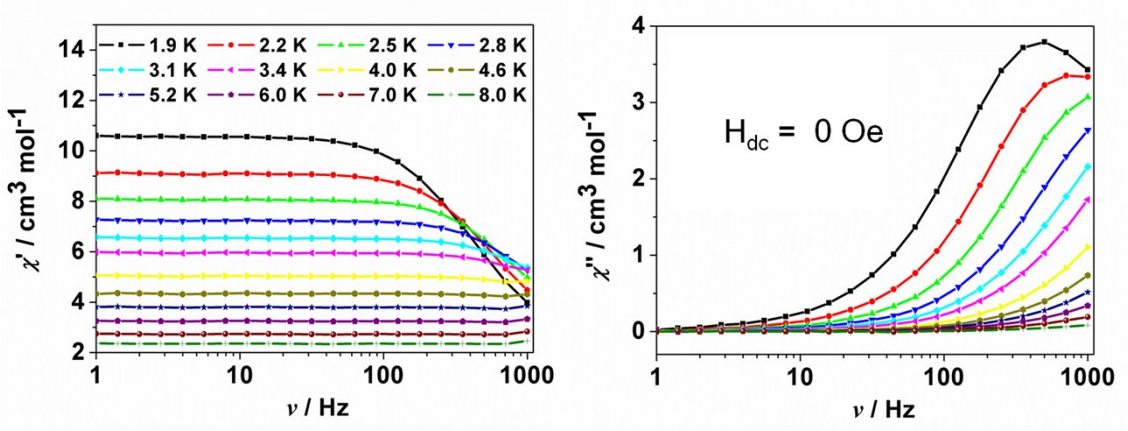

Fig. S6 Frequency-dependent in-phase χ' and out-of-phase χ'' ac susceptibility signals for **3** at the indicated temperatures under zero dc field.

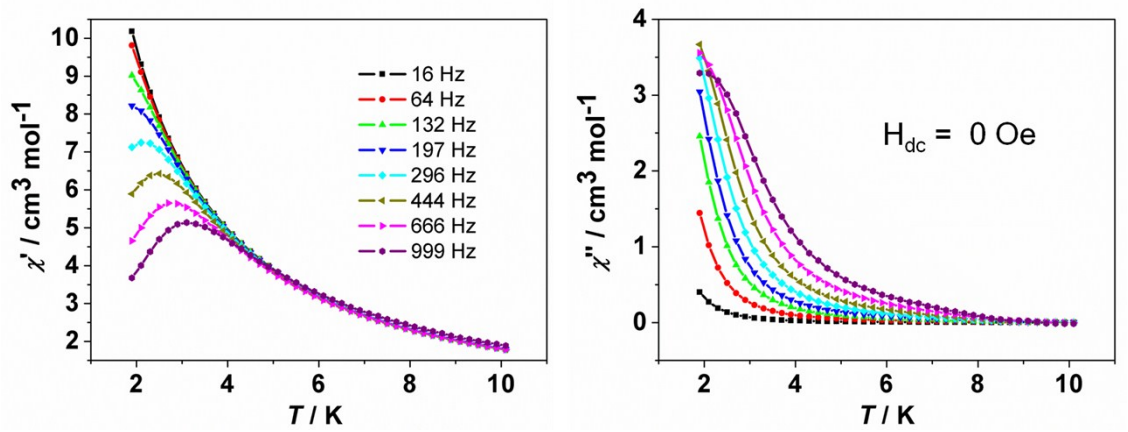

Fig. S7 Temperature-dependent in-phase χ' and out-of-phase χ'' ac susceptibility signals for **3** at the indicated frequencies under zero dc field.

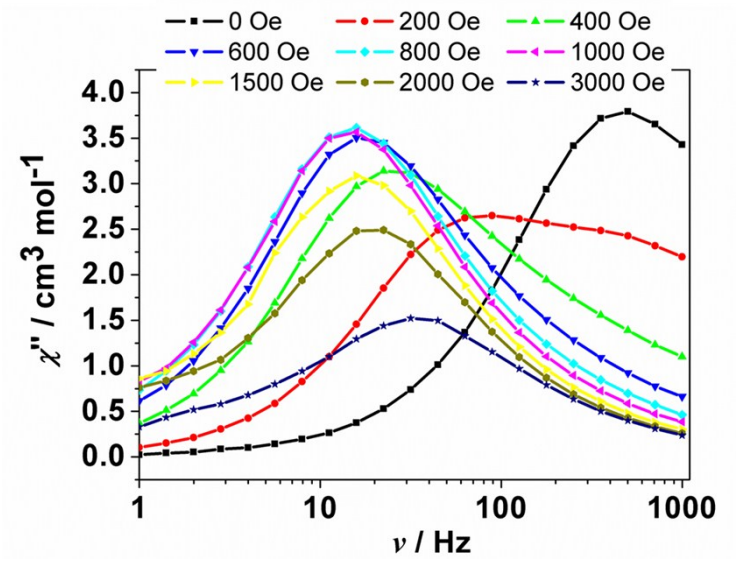

Fig. S8 Plot of out-of-phase χ'' *versus* frequency at 1.9 K for **3** under the application of variable dc fields, ranging from 0 to 3000 Oe.

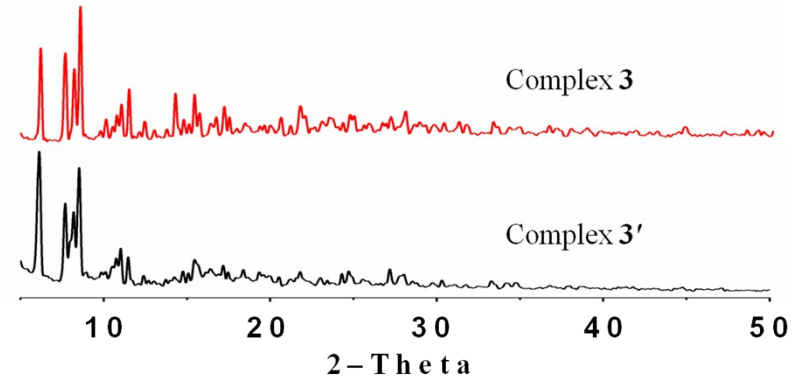

Fig. S9 The XRPD pattern of complex **3′** is consistent with that of complex **3**.

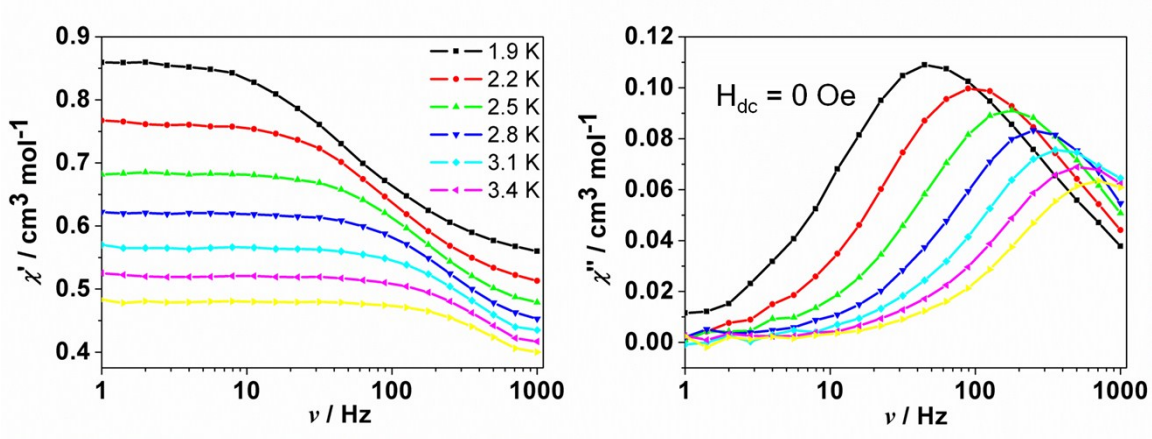

Fig. S10 Frequency-dependent in-phase χ' and out-of-phase χ'' ac susceptibility signals for **3′** at the indicated frequencies under zero dc field.

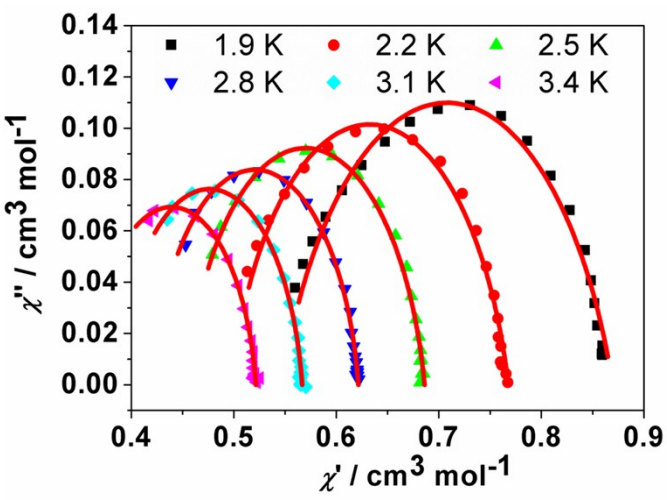

Fig. S11 Cole-Cole plots for **3′** under zero dc field. The solid lines represent the fit to the Debye model at the indicated temperatures.

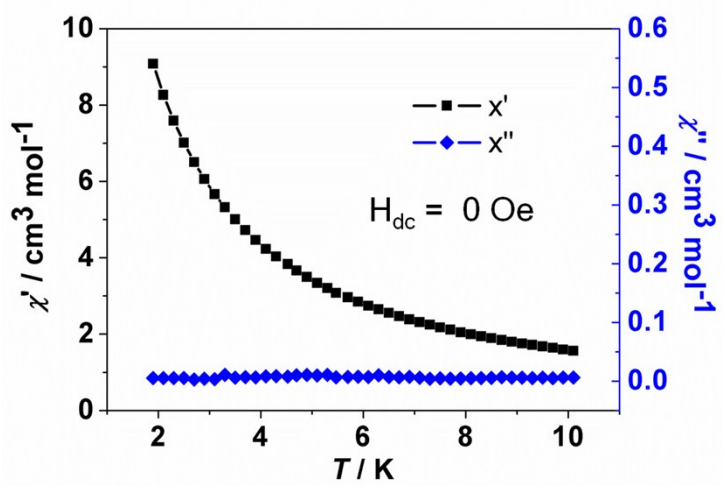

Fig. S12 Temperature-dependent in-phase χ' and out-of-phase χ'' ac susceptibility signals for **2** at the frequency of 999 Hz under zero dc field.

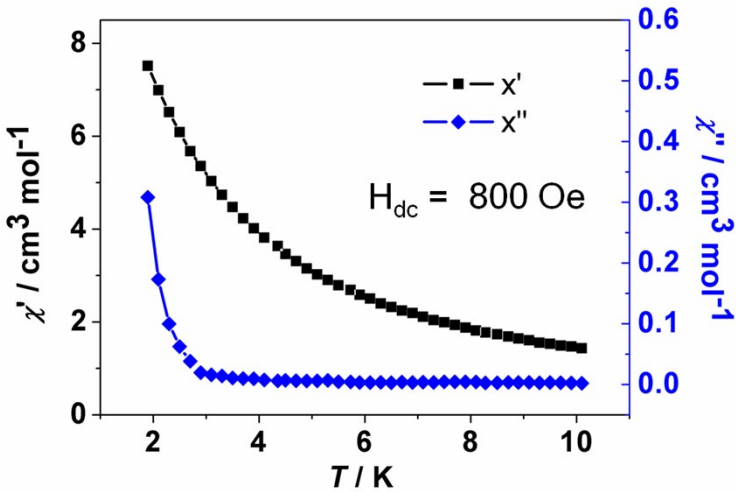

Fig. S13 Temperature-dependent in-phase χ' and out-of-phase χ'' ac susceptibility signals for **2** at the frequency of 999 Hz under 800 Oe dc field.